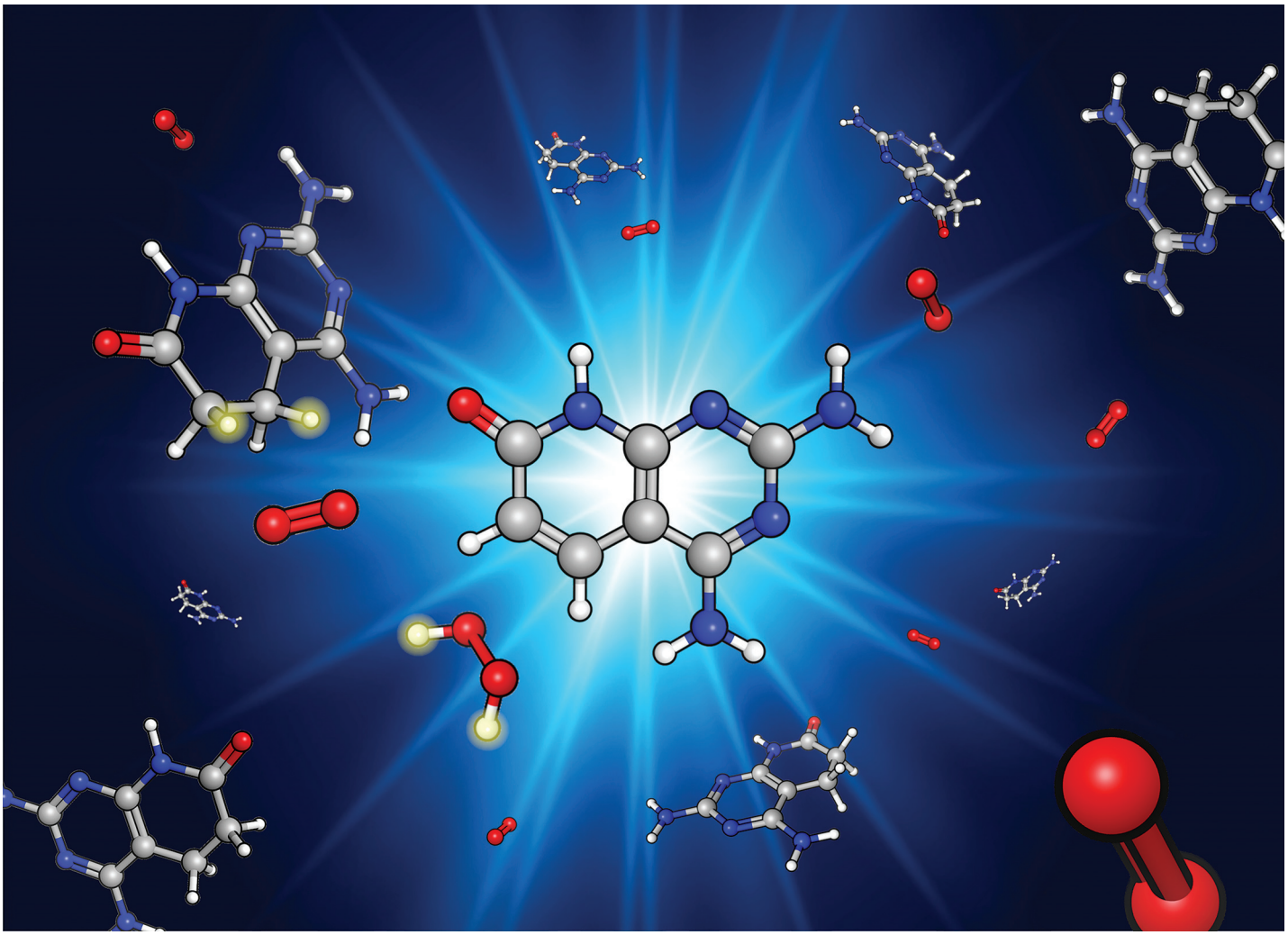

Showcasing research from Grupo de Química Farmacèutica, IQS School of Engineering, Universitat Ramon Llull, Barcelona, Spain.

Autocatalytic photoinduced oxidative dehydrogenation of pyrido[2,3-*d*]pyrimidin-7(8*H*)-ones: synthesis of C5–C6 unsaturated systems with concomitant formation of a long-lived radical

5,6-Dihydropyrido[2,3-*d*]pyrimidin-7(8*H*)-ones are dehydrogenated to the corresponding pyrido[2,3-*d*] pyrimidin-7(8*H*)-ones by irradiating at 450 or 365 nm in DMSO, in the presence of air, and at room temperature without any added photosensitizer. The picture shows the simplicity of such a process in which hydrogen peroxide is formed. Background designed by starline *via* Freepik.com.

As featured in:

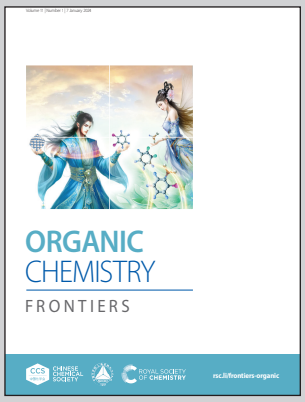

See Raimon Puig de la Bellacasa *et al.*, *Org. Chem. Front.*, 2024, **11**, 27.

CCS 中国化学会 CHINESE CHEMICAL SOCIETY
SIOC 1950
ROYAL SOCIETY OF CHEMISTRY
rsc.li/frontiers-organic

ORGANIC CHEMISTRY FRONTIERS

CCS 中国化学会 CHINESE CHEMICAL SOCIETY

SIOC 1950

ROYAL SOCIETY OF CHEMISTRY

RESEARCH ARTICLE

View Article Online
View Journal | View Issue

Cite this: *Org. Chem. Front.*, 2024, **11**, 27

Autocatalytic photoinduced oxidative dehydrogenation of pyrido[2,3-*d*]pyrimidin-7(8*H*)-ones: synthesis of C5–C6 unsaturated systems with concomitant formation of a long-lived radical†

Claudi de Rocafiguera, [a] Vega Lloveras, [b] José Vidal-Gancedo, [b] Jordi Teixidó, [a] Roger Estrada-Tejedor,[a] José I. Borrell [a] and Raimon Puig de la Bellacasa *[a]

Received 24th August 2023,
Accepted 31st October 2023

DOI: 10.1039/d3qo01358h

rsc.li/frontiers-organic

5,6-Dihydropyrido[2,3-*d*]pyrimidin-7(8*H*)-ones are readily accessed by a variety of methods and are a good scaffold for the development of biologically active compounds. However, they are very reluctant to dehydrogenate to give C5–C6 unsaturated compounds, usually with higher activity. A serendipitous discovery has allowed us to develop an autocatalytic photochemical dehydrogenation process by irradiating at 450 or 365 nm in DMSO, in the presence of air, and at room temperature the corresponding 5,6-dihydro derivative (with a variety of substituents at C2, C4, C5, C6, and N8) without adding any external photosensitizer. A complete study including reactions in DMSO-d_6 followed by NMR spectroscopy, EPR experiments, the use of radical quenchers, spin-trapping techniques, and reaction with methyl viologen, complemented with *ab initio* calculations has allowed us to propose a mechanistic rationalization for such a process.

Introduction

Our research group has been actively working in the field of Tyrosine Kinase Inhibitors (TKIs) with the aim of developing drug candidates against diverse types of cancers such as breakpoint cluster region protein (BCR) kinase inhibitors for B lymphoid malignancies,[1] discoidin domain-containing receptor 2 (DDR2) inhibitors for the treatment of lung cancer,[2] MAP kinase interacting kinase (MNK1/2) inhibitors for the treatment of breast or prostate cancer,[3] zeta-chain-associated protein kinase 70 kDa (ZAP-70) inhibitors,[4] and more recently a promising candidate for the treatment of pancreatic cancer (unpublished results).

Most of such developments are based on pyrido[2,3-*d*]pyrimidin-7(8*H*)-ones **1** (Fig. 1), a scaffold for which we have described several straightforward synthetic strategies, allowing the decoration of all the five centers of diversity present in **1**.[1,5–7]

However, some of the most versatile methodologies afford the corresponding 5,6-dihydro derivatives **2** (Fig. 1), such as the one that starts from α,β-unsaturated esters (**3**). Thus, 2-methoxy-6-oxo-1,4,5,6-tetrahydropyridin-3-carbonitriles (**5**) are obtained by the reaction of an α,β-unsaturated ester (**3**) and malononitrile (**4**) in NaOMe/MeOH.

Treatment of pyridones **5** with guanidine systems (**6**, R^2 = H, alkyl, aryl) affords 4-amino-5,6-dihydropyrido[2,3-*d*]pyrimidines (**7**, R^4 = H, alkyl, aryl). The synthesis of 2-arylamino substituted 4-amino-5,6-dihydropyrido[2,3-*d*]pyrimidin-7(8*H*)-ones (**7**, R^2 = aryl) occurred *via* the corresponding 3-aryl substituted pyridopyrimidines **8**, formed upon the treatment of pyridones **5** with an aryl-substituted guanidine **6** in 1,4-dioxane, which

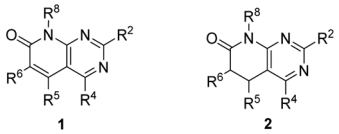

Fig. 1 Pyrido[2,3-*d*]pyrimidin-7(8*H*)-ones (**1**) and their 5,6-dihydro derivatives (**2**).

[a]*Grup de Química Farmacèutica, Institut Químic de Sarrià, Universitat Ramon Llull, Via Augusta, 390, E-08017 Barcelona, Spain. E-mail: raimon.puig@iqs.url.edu*
[b]*Institut de Ciència de Materials de Barcelona (ICMAB-CSIC) and CIBER de Bioingeniería, Biomateriales y Nanomedicina (CIBER-BBN), Instituto de Salud Carlos III, Campus UAB, E-08193 Bellaterra, Spain*

†Electronic supplementary information (ESI) available: Experimental details, characterization data, and spectra for the synthesized compounds, and the EPR and DFT calculation details. See DOI: https://doi.org/10.1039/d3qo01358h

underwent the Dimroth rearrangement to the desired 4-amino-pyridopyrimidines (**7**, R^2 = aryl) with NaOMe/MeOH. The overall yields of such a two-step protocol are in general higher than those of the reaction between pyridones **5** and an aryl-substituted guanidine **6** (Scheme 1).[5]

In those cases in which the compound obtained does not bear C5–C6 unsaturation, critical for having biological activity as TKIs, it is precise to proceed to a dehydrogenation process that has never been an easy step to be performed. We have developed useful protocols for the dehydrogenation of **2** to **1** using NaH in DMSO when an aryl substituent is present at C-6, Na_2SeO_3 in DMSO,[8] or 10% palladium on carbon in decalin at 175 °C, but these methods were highly dependent on the nature of the substituents at C5 and C6.

On the other hand, compounds **1** show a very low solubility in water and other common solvents because they are associated with a self-complementary ADAD–DADA quadruple hydrogen-bonding centrosymmetric motif. A way to increase such solubility is breaking such association by alkylation (usually methylation) of the nitrogen atom at the pyridone ring of **1**. However, in connection with a project focused on the design of TKIs against pancreatic cancer, we were interested in obtaining candidate compounds bearing an NH group at such a position. Consequently, we selected a photocleavable protecting group to ensure deprotection under smooth conditions of molecules presenting several functionalities.[9,10] More precisely, starting from 2-amino-4-phenylamino-5,6-dihydropyrido[2,3-*d*]pyrimidin-7(8*H*)-one, easily obtained by a multicomponent reaction of methyl acrylate (**3**, $R^5 = R^6 = H$), malononitrile (**4**), and *N*-phenylguanidine (**6**, R^2 = Ph) in MeOH under microwave irradiation for 10 min,[11] we obtained the protected compound **9** using 4,5-dimethoxy-2-nitrobenzyl bromide and NaH in DMSO.

When we tested the deprotection of **9** at 450 nm in DMSO, corresponding to the blue region of the spectrum recommended for the deprotection of this photolabile group,[12] surprisingly, we did not observe the elimination of the photocleavable group but the partial creation of a double bond at C5–C6, affording a mixture of **9** and **10** (Scheme 2).

Such an unexpected result, which can solve one of our main problems with our pyridopyrimidine scaffold, impelled us to study this photochemical dehydrogenation in detail. The present paper deals with the results obtained in this study.

Results and discussion

In order to determine the factors governing such dehydrogenation, we selected 2,4-diamino-5,6-dihydropyrido[2,3-*d*]pyrimidin-7(8*H*)-one (**11a**) as the model compound, which was synthesized by a multicomponent reaction of methyl acrylate (**3a**, $R^5 = R^6 = H$), malononitrile (**4**), and guanidine carbonate (**6**, R^2 = H) in MeOH under microwave (MW) irradiation at 140 °C for 10 min.[6]

The study was carried out in a Penn PhD Photoreactor M2 (Penn Photon Devices, LLC), initially provided with a 450 nm LED module, using 12 mL vials, and DMSO-d_6 as a solvent to allow the direct register of the ^{1}H-NMR spectrum of the reaction mixture. The experiments carried out are summarized in Table 1.

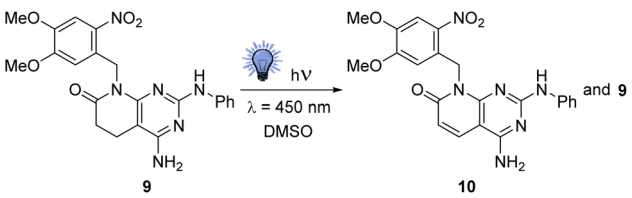

Scheme 2 Partial dehydrogenation at C5–C6 of compound **9**.

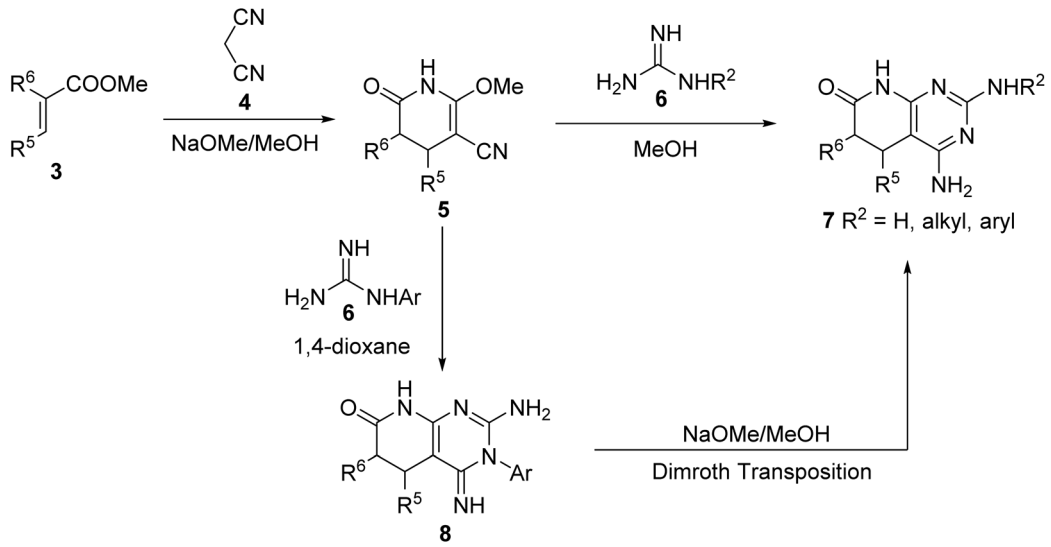

Scheme 1 Synthesis of 4-amino-5,6-dihydropyrido[2,3-*d*]pyrimidin-7(8*H*)-ones **7** from α,β-unsaturated esters **3**.

Table 1 Study of the reaction conditions for the dehydrogenation of **11a** to **12a** using blue light (λ = 450 nm) in a Penn PhD Photoreactor M2[a]

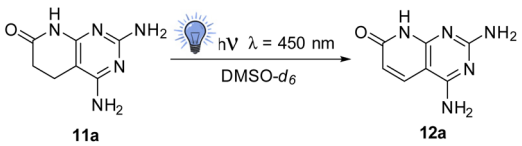

11a **12a**

Entry	Atmosphere	LED intensity (%)	Time (h)	% of **12a**[b]
1	Air, sealed vial	100	1	13
2	Air, sealed vial	100	2	22
3	Air, sealed vial	100	8	33
4	Argon, sealed vial	100	2	0
5	Oxygen, sealed vial	100	2	48
6	Oxygen, bubbling	100	1	>95
7	Oxygen, bubbling	100	2	100 + imp
8	Air, open vial	100	4	100 (76%)[c]
9	Air, open vial	0	4	0
10[d]	Air, open vial	100	2	100

[a] Reaction conditions: pyridopyrimidine **11a** (50 mg, 0.28 mmol), solvent (DMSO-d_6, 5 mL), atmosphere (as stated), LED intensity (% as stated), fan speed (6800 rpm), stirrer speed (400 rpm), time (as stated), room temperature. [b] Percentage (%) of **12a** formed, determined by relative integration of appropriate ^{1}H-NMR signals of **11a** and **12a**. [c] Isolated yield of **12a**. [d] Experiment carried out using 2 mL of DMSO-d_6.

In the first three experiments (entries 1–3), we used a sealed vial containing **11a** and DMSO-d_6 under an air atmosphere (the air initially included in the sealed vial) for 1, 2, and 8 h. The presence of **12a** in the crude reaction mixture was easily established by the presence of two doublets at 5.90 (1H) and 7.89 ppm (1H) in the ^{1}H-NMR spectrum, corresponding to H-C6 and H-C5, and a signal at 11.5 ppm (1H) corresponding to H-N8 (Fig. 2). The relative integration of these signals with respect to those of compound **11a** allows to determine the approximate percentage of **12a** in the mixture, because the reaction mixtures are extremely clean. Although the amount of **12a** in the mixture is increased with the irradiation time (from 13% in 1 h to 33% in 8 h), it seems that the conversion is limited by the amount of air (most precisely oxygen) present in the vial.

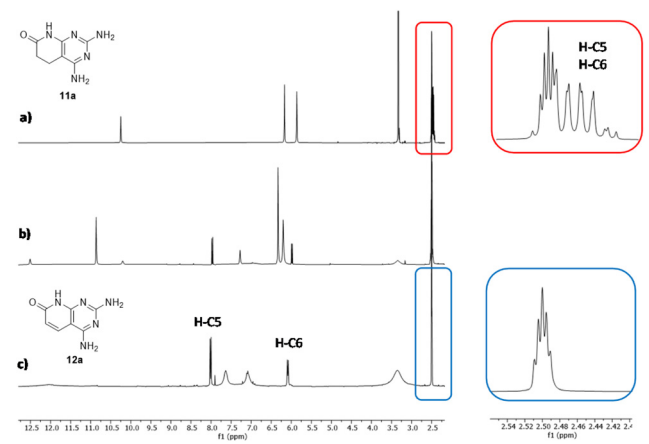

Fig. 2 Evolution of the ^{1}H-NMR spectrum of **11a** during the irradiation in a Penn PhD Photoreactor M2 (Penn Photon Devices, LLC) provided with a 450 nm LED module using DMSO-d_6 as the solvent in an open-air vial: (a) initial stage, (b) at 2 h, and (c) at 4 h.

To confirm the role of oxygen in the reaction, we repeated the experiment of entry 2, but by using a sealed vial, in which the mixture was previously bubbled with argon (entry 4), observing no dehydrogenation of **11a**.

So, we decided to repeat the experiment using a solution saturated with O_2 in a sealed vial (entry 5) also for 2 h, obtaining 48% of **12a** instead of 22% obtained when an air atmosphere was used. Consequently, we decided to carry out the experiments of entries 6 and 7 using continuous bubbling of pure O_2 for 1 h and 2 h, respectively. In both cases, the starting material was totally consumed and **12a** was formed almost quantitatively. However, in the ^{1}H-NMR spectrum of the reaction mixture at 1 h (entry 6), there were some extra signals not corresponding either to **11a** or **12a**, which could correspond to a possible reaction intermediate. These signals disappeared after two hours of irradiation (entry 7), but a plethora of small signals were formed that seemed to correspond to the over-reaction terms.

Once the critical role of the oxygen was proved, we decided to continue the experiments with a vial open to the atmosphere but provided with a $CaCl_2$ tube to prevent the entry of moisture (entries 8–10). The first experiment carried out using this approach (entry 8) afforded a total and clean conversion to **12a** after 4 h of irradiation at 450 nm. **12a** was isolated by precipitation with acetone to afford 76% yield. To confirm the need for blue light during this dehydrogenation, the previous experiment was repeated but with the LED system switched off (entry 9) and, convergently, no dehydrogenation of **11a** was observed. Finally, the amount of **11a** was doubled in entry 10 and a total conversion was obtained in only 2 h.

At this point, it is necessary to highlight that this photo-induced oxidative dehydrogenation of 5,6-dihydropyrido[2,3-*d*] pyrimidin-7(8*H*)-one **11a** is, to the best of our knowledge, the first case in which the dehydrogenation takes place without the presence of an extra photosensitizer component or metals.[13,14]

In fact, according to the work of Sadhu *et al.*,[15] most of the dehydrogenating methods use strong oxidants (H_2SO_4, HNO_3, CrO_3–acetic acid, DDQ, or MnO_2), NBS-peroxide assisted oxidation, or metal catalysts ($Cu(OAc)_2$–$Pb(OAc)_4$ and Pd–C). Their photochemical dehydrogenation using oxygen and a photo-induced electron transfer (PET) sensitizer (9-cyanoanthracene, 9-cyanophenanthrene, or 1-cyanonaphthalene) is the only precedent of our autocatalytic process.

Once the best reaction conditions were found and the key role of oxygen and light was established in the dehydrogenation of **11a**, we decided to evaluate the effect of the presence of substituents at positions C5 and C6 and the impact of changing the wavelength of the used light by using a complementary 365 nm LED module. Consequently, we synthesized compounds **11b–e** (Scheme 3), starting from the corresponding

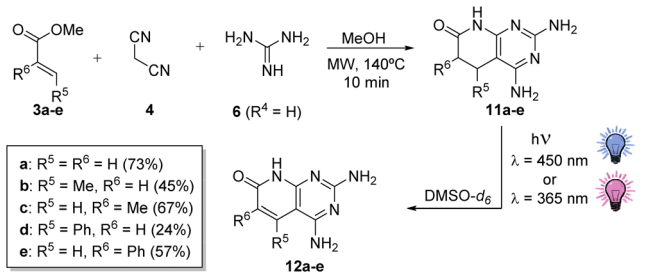

Scheme 3 Synthesis of 5,6-dihydropyridopyrimidines **11b–e** with substituents at C5 or C6 and subsequent photochemical dehydrogenation to **12b–e** and their isolated yields.

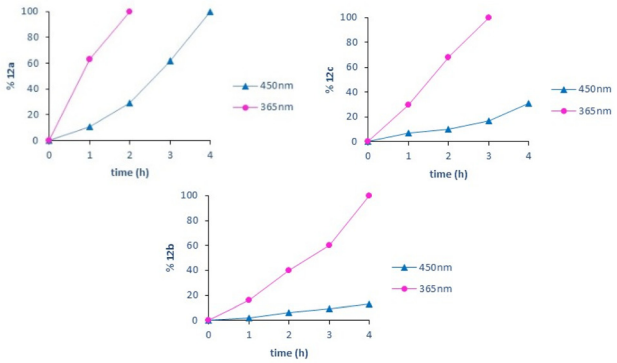

Fig. 3 Kinetic curves for the dehydrogenation of **11a–c** at 450 and 365 nm using bubbled air in an open vial.

α,β-unsaturated esters (**3b–e**), malononitrile (**4**), and guanidine carbonate (**6**·H_2CO_3, R^2 = H), using the multicomponent protocol previously developed by our group.[11]

We decided to start the study using **11c** (R^5 = H, R^6 = Me), the compound presenting a methyl at the α-carbonyl position, because substitution at position C6 is usually connected with better TKI activities. The assay was carried out by using 0.26 mmol of **11c** in 2 mL of DMSO-d_6, at 450 nm with 100% LED and a fan at 6800 rpm, in an open-air vial provided with a $CaCl_2$ tube as in the case of **11a**.

After 4 h of irradiation, the conversion to **12c** (R^5 = H, R^6 = Me) was complete, as proved in the ^{1}H-NMR spectrum (see the ESI†) by the presence of a singlet (1H) at 7.86 ppm corresponding to H-C5 and a singlet (3H) at 1.98 ppm of Me-C6. The isolated yield upon precipitation with acetone was 64%. The results were similar at 365 nm. In contrast, in the case of **11b** (R^5 = Me, R^6 = H), after 2 h of irradiation at 450 and 365 nm, the conversions to **12b** were 1% and 22%, respectively, seeming to indicate faster kinetics at 365 nm. After reducing the initial amount of **11b** to 0.051 mmol to ensure the completion of the reaction, the total conversion to **12b** was possible only after 3 h of irradiation at 365 nm, although with minor impurities, while at 450 nm, there was still **11b** without any reaction. The isolated yield of **12b** at 365 nm upon precipitation with acetone was 45% (^{1}H-NMR spectrum: 5.77 ppm (s, 1H) H-C6; 2.5 ppm (s, 3H) Me-C5).

These results seemed to indicate that the kinetics of the reaction were favored at 365 nm. To better compare the results at both wavelengths excluding a possible different diffusion process of the air into the vial between experiments, we decided to bubble compressed air into the vial in the forthcoming reactions. Using in all cases 0.26 mmol of the corresponding **11a–c**, the reactions were carried out at 450 and 365 nm, taking samples each hour until a maximum of 4 h. The percentage of the resulting dehydrogenation compounds **12a–c** was obtained by relative integration in the corresponding ^{1}H-NMR spectrum. The kinetic curves for the dehydrogenation process conducted in this way (Fig. 3) show that the dehydrogenation proceeds faster at 365 nm than at 450 nm (this aspect will be discussed later in this paper).

Taking this result into account, we carried out the dehydrogenation of **11e** (R^5 = H, R^6 = Ph) and **11d** (R^5 = Ph, R^6 = H) using 0.26 mmol in DMSO-d_6 and 100% LED intensity at 365 nm and bubbling air into the sample. Under these conditions, **11e** needed 7 h for the complete conversion in **12e** (characterized by a singlet, 1H at 8.25 ppm corresponding to the H-C5 proton), while **11d** needed 10 h to achieve the same result (in this case, H-C6 appears at 5.69 ppm), but the impurity level was clearly higher. Such results clearly showed that the ease of dehydrogenation depends on the nature and position of the substituents present on the pyridone ring, being better when smaller in size and when the substituent is present at C6.

With all the preceding results in hand, we began to consider proposing a mechanistic rationalization able to explain the above observations. We took the mechanism proposed by Schilling *et al.*[16] for the visible-light-induced oxidation of benzyl alcohol to benzaldehyde with oxygen in DMSO and blue light in the presence of 9-fluorenone as a referable and plausible starting point for our proposal.

Consequently, we evaluated the effect of several quenchers in the conversion of **11a** (R^5 = R^6 = H) to **12a** (Table 2) to recognize the reactive oxygen species. The use of sodium azide does not affect the conversion to **12a**, thus revealing that singlet oxygen is not formed or at least has no role in the dehydrogenation. In contrast, the strong effect of benzoquinone clearly indicates that the superoxide radical anion ($O_2^{\bullet-}$) plays a major role in this process. Spin trapping studies (discussed

Table 2 Quenching experiments for the dehydrogenation of **11a** to **12a** using blue light (λ = 450 nm) in a Penn PhD Photoreactor M2[a]

Quencher	Equivalent	% of **12a**[b]	Type of scavenger
NaN_3	10	100	Singlet oxygen scav.
BHT	1.0	7	Radical scav.
Benzoquinone	1.0	4	Superoxide radical anion scav.
$CuCl_2$	1.0	20	Electron scav.
t-BuOH	1.0	100	Hydroxyl radical scav.

[a] Reaction conditions: 0.14 mmol of **11a**, DMSO-d_6 (1.0 mL), air bubbling in an open vial. [b] Percentage (%) of **12a** formed determined by relative integration of appropriate ^{1}H-NMR signals of **11a** and **12a**.

later in this paper, see the ESI, pages S42 and S43†) confirmed such an assumption. The quenching effect on the conversion to **12a** of BHT, and to a lesser extent of $CuCl_2$, suggests the interplay of a radical in this process. However, the fact that the addition of *t*-BuOH has no effect on the transformation excludes the participation of the hydroxyl radical in the transformation of **11a** to **12a**.

Complementarily, we studied the effect of TEMPO (2,2,6,6-tetramethyl-1-piperidinyloxy, free radical) on the dehydrogenation of **13** to **14** (Scheme 4). **13** (obtained following the protocol described by Galve *et al.*[6]) was selected as a substrate to increase the solubility, and to allow the analysis of the resulting crude mixture by HPLC-MS, as the use of ^{1}H-NMR is not possible due to the presence of a radical species. When the reaction was carried out in the absence of TEMPO using blue light (λ = 450 nm) and DMSO-d_6 as a solvent in the presence of air, the dehydrogenation took place in 1 h, affording 73% of **14** (structure confirmed by MS). In contrast, in the presence of TEMPO, the conversion to **14** was reduced to 6% after 1 h of irradiation, proving once more the radical character of such dehydrogenation.

Once the key role of the superoxide radical anion ($\mathbf{O_2^{\bullet-}}$) in the process was established and the formation of H_2O_2 was expected during the dehydrogenation, we tested the presence of such a compound by adding NaI/AcOH during the irradiation of **11e** (R^5 = H, R^6 = Ph) and observed the evolution of a brownish color corresponding to the I_2 formed that was decolorized by the addition of sodium thiosulfate. Knowing that the evolution of H_2O_2 in DMSO causes the oxidation of the latter to dimethyl sulfone ($CH_3SO_2CH_3$), we concentrated the DMSO of one of the experiments and recorded both the ^{1}H- and ^{13}C-NMR spectra, observing the characteristic signals of dimethyl sulfone at 2.99 and 42.1 ppm, respectively, thus confirming the formation of such an oxidation compound of DMSO.

To evaluate if the starting pyridopyrimidine can form one of the radicals involved in the process, we decided to use methyl viologen dichloride hydrate to test, in the absence of oxygen, whether the pyridopyrimidine structure can give electrons to such dyestuff, reducing it to the blue colored form. When the reaction was carried out with **11e** (R^5 = H, R^6 = Ph) in DMSO degasified with argon at 450 nm for 30 min, the initially pale-yellow solution changed to dark blue, confirming the transference of electrons from **11e** to methyl viologen. No color was observed in the presence of air. Such a result could be considered an indirect confirmation of the Single Electron Transfer (SET) from the excited state **[11e]*** to methyl viologen, forming the corresponding cation-radical $\mathbf{[11e]^{\bullet+}}$.

Scheme 4 Inhibition by TEMPO of the dehydrogenation of **13** to **14**.

At this point of the mechanistic study, we decided to use electron paramagnetic resonance (EPR) spectroscopy, a specific technique to characterize radicals,[17,18] to gain more insight into the radicals involved in this process. The experiment carried out consisted of recording the EPR spectrum of a sample of the dehydrogenation of **11a** (R^5 = R^6 = H) to **12a**, at a concentration of 25 mg mL^{-1} in DMSO-d_6 after 15 min of irradiation at 450 nm with bubbling of air. The result was the spectrum included in Fig. 4a, corresponding to a highly stable radical species that can be directly detected without the use of a spin trap, which presents eleven groups of lines. The EPR spectrum was simulated by using Bruker WIN-EPR SimFonia software (Fig. 4b) and it is compatible with the experimental one considering 5 quasi-equivalent N atoms (I = 1), 3 N atoms with a hyperfine coupling constant (hfcc) of 1.67 G and 2 N atoms with a hfcc of 1.69 G, to simulate the basic EPR pattern.

This could indicate an important delocalization of the spin density over the 5 nitrogen atoms of **11a**. The fine structure of each group of the eleven lines was compatible with 4 equivalent H with a hfcc of 0.32 G and another H with a constant of 0.15 G. The *g*-factor and linewidth were g = 2.00445 and ΔH_{pp} = 0.1 G, respectively. The spectrum obtained was identical if non-deuterated DMSO was used.

When the spectrum was recorded at 15, 30, 45, 60, and 75 min of irradiation, a decrease in the EPR signal was observed. However, such a radical was still observed after 1 month, showing its great stability. Such a radical could be the cation radical of the starting material **11a** ($\mathbf{[11a]^{\bullet+}}$). The transference of a hydrogen radical and a proton from the first to the second would explain the formation of the C5–C6 double bond and the concomitant production of H_2O_2.

With the aim of obtaining more information about the nature of the radicals involved in the process, we decided to use the spin trapping technique using DMPO (5,5-dimethyl-1-pyrroline *N*-oxide).[19] Such a spin trap reacts with radical species to form a stable radical adduct that allows to characterize the atom that has been bonded to the DMPO β-carbon atom (with respect to the oxygen atom) based on the H_β coupling constant. If such a coupling constant is smaller than 20 G,

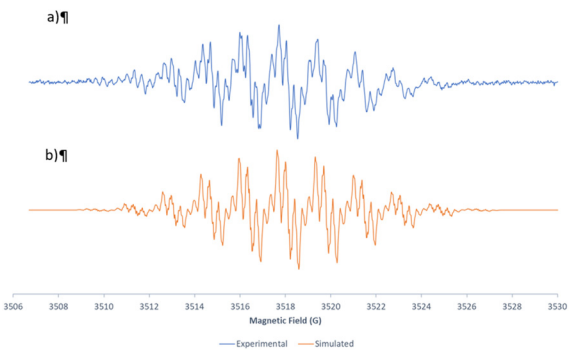

Fig. 4 Experimental (a) and simulated (b) EPR spectra corresponding to the radical species formed during the dehydrogenation of **11a** to **12a** at 450 nm using bubbled air in an open vial.

the atom linked to the DMPO carbon is an oxygen atom (OCR, oxygen centered radical) and if it is greater than 20 G, the linked atom is a carbon atom (CCR, carbon centered radical).

When we irradiated a mixture of **11a** and DMPO in DMSO-d_6 with bubbling of air at 450 nm for 30 min, the EPR spectrum (see the ESI, page S42†) showed 2 groups of lines: a group of 3 main lines, which corresponded to a DMPO impurity that was already present in the blank spectrum of the DMPO used, and a second group composed of 4 groups of lines, whose coupling constants obtained from the simulation were a_N = 13 G, a_{H_β} = 10.4 G and a_{H_γ} = 1.35 G with a linewidth of 0.7 G and a *g*-factor of 2.0056.

This DMPO radical adduct spectral pattern was compatible with the trapping of the superoxide radical anion ($\mathbf{O_2}^{\bullet-}$), thus confirming the main role of such species in the dehydrogenation process.

In contrast, when we carried out such an experiment by adding an excess of DMPO to the radical already formed from **11a** after 30 min of irradiation at 450 nm with bubbling of air, we obtained an EPR signal (see the ESI, page S43†) with a H_β coupling constant of 20.8 G, compatible with an adduct of DMPO, and the cation radical $\mathbf{[11a]}^{\bullet+}$ through a carbon atom.

DFT calculations using Gaussian 16 at the B3LYP/6-311++G(d,p) theory level of the cation-radical $\mathbf{[11a]}^{\bullet+}$ of **11a** were carried out (Fig. 5).

Such calculations showed that in the case of the cation-radical $\mathbf{[11a]}^{\bullet+}$, the radical was centered on the C4a bridgehead carbon and the spin density delocalized on the five nitrogen atoms, in accordance with the EPR data (Fig. 6).

Having apparently identified all the pieces of the reaction mechanism, that is, the starting product **11a**, its excited state $\mathbf{[11a]}^*$, the cation-radical $\mathbf{[11a]}^{\bullet+}$, oxygen in the ground state ($^3\mathbf{O_2}$) and the superoxide radical anion ($\mathbf{O_2}^{\bullet-}$), the final dehydrogenated product **12a**, and H_2O_2, before proposing such a mechanism, the DFT calculations of all species involved using Gaussian 16 were performed at the B3LYP/6-311++G(d,p) theory level (TD-DFT for the excited state $\mathbf{[11a]}^*$) with DMSO as an implicit solvent (Table 3). As a result of such calculations, the reaction mechanism included in Scheme 5 was proposed.

We propose the excitation of **11a** ($R^5 = R^6 = H$) to the excited state $\mathbf{[11a]}^*$. The excited state could be achieved at 450 nm (which corresponds to an energy contribution of 63.5 kcal mol^{-1}), but was certainly easier at 365 nm (corresponding to 78.3 kcal mol^{-1}), thus explaining the observed faster kinetics at this wavelength. Such an excited state $\mathbf{[11a]}^*$ would suffer a Single Electron Transfer (SET) to oxygen with the corresponding formation of the cation-radical $\mathbf{[11a]}^{\bullet+}$ and superoxide radical anion ($\mathbf{O_2}^{\bullet-}$). Such direct transfer is energetically favorable when the calculation includes DMSO as an implicit solvent (−36.9 kcal mol^{-1}).

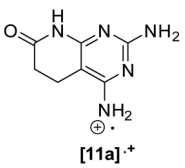

Fig. 5 Cation-radical $\mathbf{[11a]}^{\bullet+}$ of **11a**.

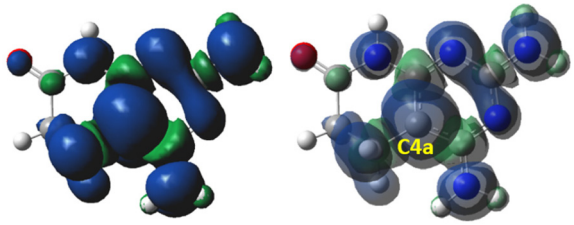

Fig. 6 Spin density of the cation-radical $\mathbf{[11a]}^{\bullet+}$ (below) of **11a** calculated using Gaussian 16 at the B3LYP/6-311++G(d,p) theory level, showing delocalization on the five nitrogen atoms present in $\mathbf{[11a]}^{\bullet+}$ but centered on the C4a bridgehead carbon.

Table 3 Energy (Hartrees) calculated for the different species involved in the mechanism of dehydrogenation of **11a** to **12a** in DMSO (using a CPCM implicit solvent model)[a]

Structure	Role	Implicit DMSO[b]
11a	Starting compound	−621.410320
$^3\mathbf{O_2}$	Oxygen	−150.370631
$\mathbf{[11a]}^*$	Excited state	−621.277098
$\mathbf{[11a]}^{\bullet+}$	Cation-radical	−621.197657
$\mathbf{O_2}^{\bullet-}$	Superoxide radical anion	−150.504930
$^1\mathbf{O_2}$	Singlet oxygen	−150.310000
$\mathbf{HOO}^-$	Hydrogen peroxide anion	−151.117206
15a	Intermediate tautomer	−620.616069
12a	Final compound	−620.202291
$\mathbf{H_2O_2}$	Hydrogen peroxide	−151.610302

[a] DFT calculations using Gaussian 16 were performed at the B3LYP/6-311++G(d,p) theory level (TD-DFT for the excited state $\mathbf{[11a]}^*$). [b] An implicit DMSO solvent model calculated using the CPCM method.

Although the formation of the superoxide radical anion ($\mathbf{O_2}^{\bullet-}$) seems to be clear, taking into account the quenching experiments included in Table 2 and the favorable energy associated with the SET between the excited state of **11a** and oxygen obtained in the DFT calculations, we cannot exclude the concomitant formation of other Reactive Oxygen Species (ROS) such as singlet oxygen ($^1\mathbf{O_2}$), although it was not detected in our experiments.

The resulting radical-cation $\mathbf{[11a]}^{\bullet+}$ and superoxide radical anion ($\mathbf{O_2}^{\bullet-}$) pair would evolve by a radical hydrogen abstraction at C5 with the formation of the HOO^- anion and a C4a–C5 double bond affording **15a**. The predicted high spin density at C4a of $\mathbf{[11a]}^{\bullet+}$ would favor the abstraction of the hydrogen radical and the concomitant formation of the C4a–C5 double bond. The final tautomerization through the abstraction of a proton at C6 of **15a** by the HOO^- anion would afford the final dehydrogenated compound **12a** and H_2O_2. Such tautomerization is favored by a decrease of the pK_a value of the α-carbonyl methylene group due to the presence of the C5–C4a formed double bond (from around 20–25 to 9.6, value

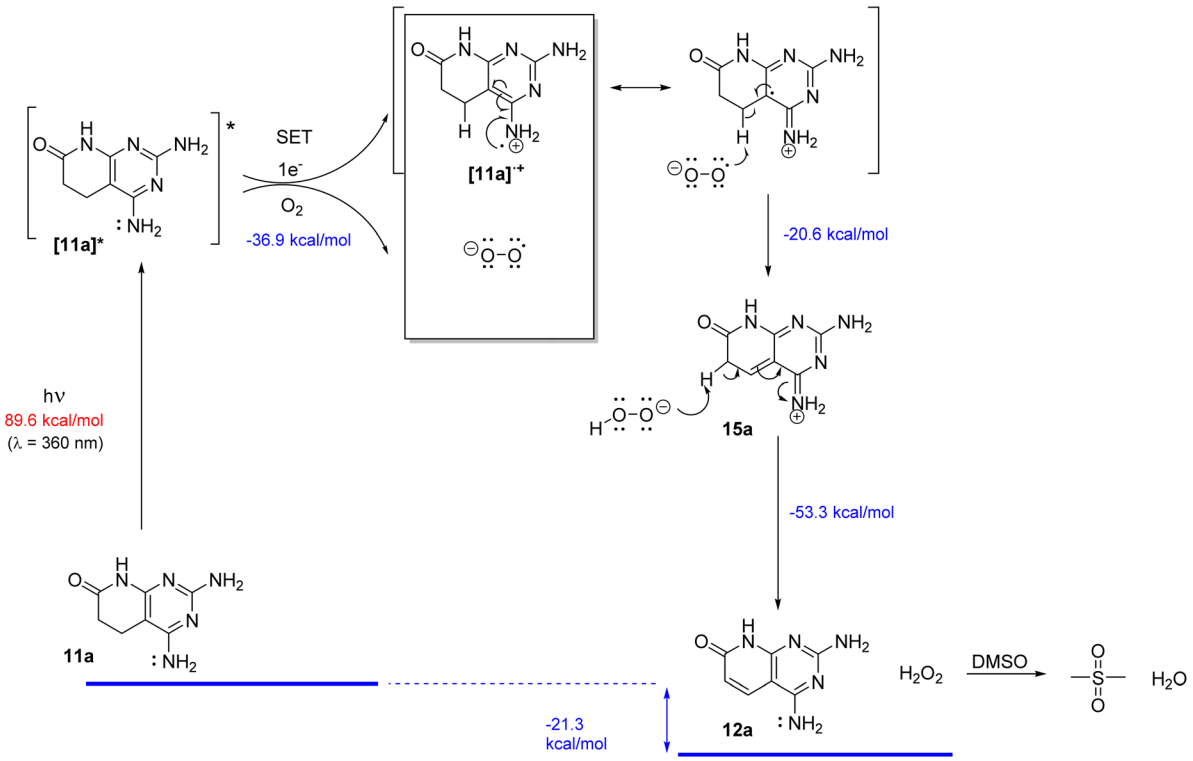

Scheme 5 Proposed reaction mechanism for the dehydrogenation of **11a** to **12a** in DMSO irradiated with light (450 or 365 nm) in the presence of oxygen.

predicted for **15a** with Marvin version 21.18.0, ChemAxon, https://www.chemaxon.com). The generated H_2O_2 oxidizes DMSO to dimethyl sulfone.

Such a mechanistic proposal is also useful to understand the dehydrogenation of compounds **11b–e** that present substituents at R^5 or R^6 and is also capable of rationalizing why the reaction is slower when there is a substituent at R^5 either by steric hindrance that it can cause or by the fact that there is only one hydrogen atom to be abstracted from such a position. However, all the compounds **12a–e** studied to date have two amino groups at C2 and C4 and an unsubstituted nitrogen atom at N8. In order to determine if such dehydrogenation can take place in other pyrido[2,3-*d*]pyrimidine scaffolds, we decided to synthesize the compounds included in Chart 1.

Thus, compound **16** was synthesized in 10% yield from methyl acrylate and guanidine using the procedure previously described by our group.[11] Compound **17** was obtained from methyl acrylate and 6-amino-2-(methylthio)pyrimidin-4(3*H*)-one in 25% yield using an extension of the protocol described also by our group.[7] **18** was obtained in 49% yield following the protocol described in Scheme 1, starting from methyl 2-(4-fluorophenyl)acrylate.[5,6] Finally, compound **19** was obtained in 91% yield from **11a** upon treatment with 10 equiv. of NaH and 10 equiv. of MeI.

Compounds **16–19** were dehydrogenated at 365 nm to the corresponding compounds **20–23** bearing a C5–C6 double

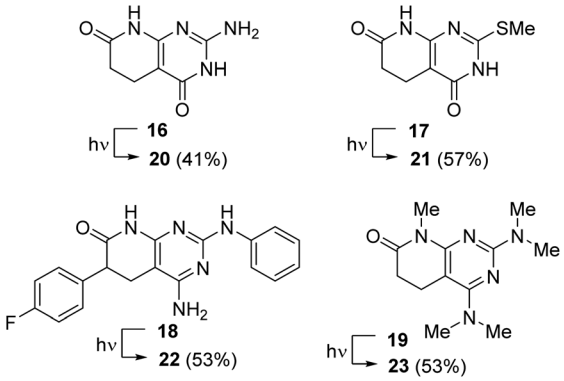

Chart 1 Complementary compounds **16–19** evaluated in the dehydrogenation with light (450 or 365 nm) in the presence of air. The corresponding C5–C6 unsaturated compounds are **20–23**.

bond after 2.5, 5 and 10 h starting from 0.13, 0.13, and 0.07 mmol, respectively, thus showing an increased difficulty in such dehydrogenation. Although the conversions were almost quantitative, the isolated yields upon precipitation were 41%, 57%, and 53%. The use of a 450 nm lamp in the case of **16** increased the irradiation time to 8 h, also increasing the impurities present.

On the other hand, with the aim of evaluating whether DMSO is the only solvent adequate for such a process, we

selected compounds **11e** (R^5 = H, R^6 = Ph) and **13** to be irradiated at 365 nm in DMF and acetone, respectively, with bubbling air. **11e** was converted into **12e** in DMF in 2 h, affording an isolated 45% yield. Similarly, 0.2 mmol of **13** in acetone was dehydrogenated to **14** in 2 h, affording the final isolated compound in 74% yield. In contrast, no dehydrogenation was achieved in a proton-active solvent such as MeOH. These results seem to confirm that DMSO used in our study has no key role in the process either as a photocatalyst or a stabilizer.

Finally, the pentamethyl substituted compound **19** was dehydrogenated in DMSO at 365 nm in 1 h to afford compound **23** in 53% yield. The dehydrogenation achieved with **19** is especially relevant in supporting the proposed mechanism, in particular, the suggested formation of the C4a–C5 double bond by the radical abstraction of the H-C5 hydrogen, because in this case all nitrogen atoms are methylated, so without having any hydrogen bonded to an heteroatom, the mechanism must necessarily pass through the abstraction of the aforementioned H-C5.

A last aspect to be considered for our process was the difference in the kinetics at 450 and 365 nm. Although the energy calculated for the excitation of **11a** to **[11a]*** (79.3 kcal mol^{-1}) seems to adequately fit with the energy given by the irradiation at 365 nm (78.3 kcal mol^{-1}), we wanted to analyze if there could be another hidden factor. Consequently, we recorded the UV-visible spectra of **11a** and **12a** (Fig. 7) and we realized that the absorption both at 450 and 365 nm for **11a** was extremely low, but apparently enough for the reaction to proceed.

We determined the molar absorptivity of each compound, by measuring the absorption at three different concentrations, obtaining 11 857 L mol^{-1} cm^{-1} for **12a** and 6856 L mol^{-1} cm^{-1} for **11a**. These results agree with the higher conjugation observed in **12a** due to the introduction of the extra double bond. The fact that the two absorption spectra crossed at certain wavelengths could indicate the presence of isosbestic points during the dehydrogenation process.

Consequently, the UV-visible spectrum of the reaction mixture was recorded each 15 min from 0 to 120 min (Fig. 8), showing two isosbestic points at 280 and 301 nm. The existence of isosbestic points in a chemical process indicates that there are no secondary reactions, and the absence of new

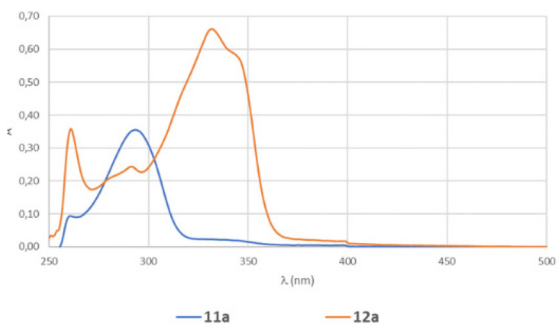

Fig. 7 UV-visible spectra of **11a** and **12a**.

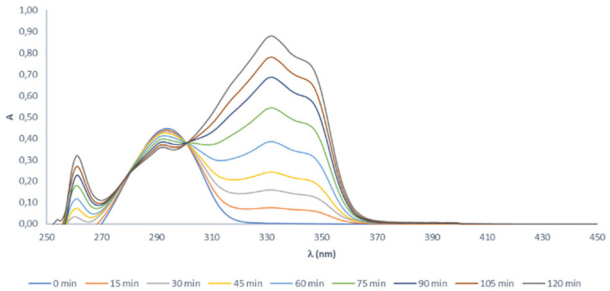

Fig. 8 UV-visible spectrum of the reaction medium recorded each 15 min.

absorption maxima, different from that of the starting product and that of the final compound, also indicates that there are no reaction intermediates that coexist long enough to absorb.

However, the fact that the absorption of **12a** at 365 nm is extremely high led us to consider the possible formation of the radical of such a compound during the dehydrogenation process at such a wavelength and its possible role as a photosensitizer, thus increasing the kinetics of the reaction. Consequently, we irradiated **12a** in DMSO-d_6 in the presence of bubbling air and at 450 nm for 30 min and we registered the EPR spectrum obtaining an EPR signal (not as well resolved as in the case of **11a** due to the lower solubility of **12a** in DMSO), which proved that **12a** can also form a radical with enough stability to be detected.

On the other hand, we conducted the normal dehydrogenation of **11a** in DMSO at 365 nm, adding a 10% molar amount of **12a** to see if there is a possible role of the latter compound as a photosensitizer, which increases the kinetics of the reaction, but we did not see a significant reduction of the reaction time.

Finally, we have also demonstrated that this methodology can be scaled-up. Starting from 1.0 g (5.6 mmol) of **11a** in 40 mL of DMSO and irradiating the solution at 365 nm for 43 h, we achieved complete dehydrogenation and the isolation of **12a** with a 76% yield.

Conclusions

In conclusion, a serendipitous discovery has allowed us to develop a general and clean method for the dehydrogenation of 5,6-dihydropyrido[2,3-*d*]pyrimidin-7(8*H*)-ones with a wide range of different substituents at C2, C4, C5, C6, and N8 by using the irradiation in DMSO (or other non-protic solvents) at 450 or 365 nm (the latter with shorter reaction times) in the presence of bubbling air and at room temperature. This reaction occurs without the addition of any photosensitizer because the pyridopyrimidine scaffold acts like it in an autocatalytic process that, to the best of our knowledge, is the first ever described in the literature for a dehydrogenation of a pyridone ring.

A mechanistic proposal has been established based on experiments carried out in DMSO-d_6, followed by NMR spectroscopy, EPR experiments, use of radical quenchers, spin-trapping techniques, and reaction with methyl viologen. Such experiments allowed us, in the case of the dehydrogenation of the C5–C6 unsubstituted compound **11a** to **12a**, to establish the radical nature of the process and detect using EPR a radical extended to the 5 nitrogen atoms of the pyridopyrimidine structure that was assigned to be the corresponding radical-cation **[11a]**$^{\bullet+}$ on the basis of the DFT calculations. Computational predictions also indicated that such a radical was mainly centered at C4a (the bridgehead carbon between C5 and N4). Convergently, the treatment of this radical with DMPO yielded a radical adduct, which indicated the trapping of a carbon centered radical, probably by binding of C4a to DMPO. The studies carried out with radical quenchers have clearly indicated the key role of the superoxide radical anion ($\mathbf{O_2}^{-}$) in such a process, and its conversion in hydrogen peroxide that later transform DMSO to the corresponding dimethyl sulfone ($DMSO_2$).

All these pieces of experimental evidence and the DFT calculations carried out in implicit DMSO have allowed us to propose a mechanism that starts with the absorption of one photon by **11a** molecules to yield the corresponding excited state **[11a]***, which suffers a SET process with oxygen to yield the corresponding radical-cation **[11a]**$^{\bullet+}$ and the superoxide radical anion ($\mathbf{O_2}^{\bullet-}$), which abstracts a hydrogen radical probably from C5 of the radical-cation **[11a]**$^{\bullet+}$ to give hydrogen peroxide anion ($\mathbf{HOO}^{-}$) and a C5–C4a unsaturated intermediate that finally undergoes a proton abstraction at C6 to yield hydrogen peroxide ($\mathbf{H_2O_2}$) and the final C5–C6 unsaturated compound **12a** through a tautomeric process.

Author contributions

The manuscript was written through contributions of all authors. All authors have given approval to the final version of the manuscript. C. d. R., investigation; V. L., investigation; J. V.-G., investigation and methodology; J. T., formal analysis; R. E.-T., investigation; J. I. B., conceptualization and writing – original draft; R. P. d. l. B., conceptualization and supervision.

Conflicts of interest

There are no conflicts to declare.

Acknowledgements

This research was funded by Ministerio de Ciencia, Innovación y Universidades, Proyectos de I + D + I "Retos Investigación" del Programa Estatal de I + D + I orientada a los Retos de la Sociedad, grant number RTI2018-096455-B-I00. We thank Dr Alexandr Shafir of the Institute of Advanced Chemistry of Catalonia (IQAC-CSIC) and Dr Ana Belén Cuenca of Institut Químic de Sarrià, Universitat Ramon Llull for giving us the possibility of carrying out the first experiment using Penn PhD Photoreactor M2. We thank one of the referees for very interesting and fruitful suggestions and discussion about the mechanistic proposal.

References

1 R. Puig de la Bellacasa, G. Roué, P. Balsas, P. Perez-Galan, J. Teixido, D. Colomer and J. I. Borrell, 4-Amino-2-arylamino-6-(2,6-dichlorophenyl)-pyrido[2,3-*d*]pyrimidin-7-(8*H*)-ones as BCR kinase inhibitors for B lymphoid malignancies, *Eur. J. Med. Chem.*, 2014, **86**, 664–675.

2 M. A. Molina, S. García-Román, J. I. Borrell, J. Teixidó, R. Estrada-Tejedor and R. Puig de la Bellacasa, *(2,6-dichlorophenyl)-8-methyl-2-(phenylamino)-pyrido[2,3-*d*]pyrimidin-7(8*H*)-one for treatment of solid cancers*, EP3120851A1, 2017.

3 E. Bou-Petit, S. Hümmer, H. Alarcon, K. Slobodnyuk, M. Cano-Galietero, P. Fuentes, P. J. Guijarro, M. J. Muñoz, L. Suarez-Cabrera, A. Santamaria, R. Estrada-Tejedor, J. I. Borrell and S. R. y. Cajal, Overcoming Paradoxical Kinase Priming by a Novel MNK1 Inhibitor, *J. Med. Chem.*, 2022, **65**, 6070–6087.

4 V. Masip, Á. Lirio, A. Sánchez-López, A. B. Cuenca, R. Puig de la Bellacasa, P. Abrisqueta, J. Teixidó, J. I. Borrell, A. Gibert and R. Estrada-Tejedor, Expanding the Diversity at the C-4 Position of Pyrido[2,3-*d*]pyrimidin-7(8*H*)-ones to Achieve Biological Activity against ZAP-70, *Pharmaceuticals*, 2021, **14**, 1311.

5 I. Galve, R. Puig de la Bellacasa, D. Sanchez-Garcia, X. Batllori, J. Teixido and J. I. Borrell, Synthesis of 2-arylamino substituted 5,6-dihydropyrido[2,3-*d*]pyrimidine-7(8*H*)-ones from arylguanidines, *Mol. Diversity*, 2012, **16**, 639–649.

6 I. Galve, R. Ondoño, C. de Rocafiguera, R. Puig de la Bellacasa, X. Batllori, C. Puigjaner, M. Font-Bardia, O. Vallcorba, J. Teixidó and J. I. Borrell, A captured room temperature stable Wheland intermediate as a key structure for the orthogonal decoration of 4-amino-pyrido[2,3-*d*]pyrimidin-7(8*H*)-ones, *Org. Biomol. Chem.*, 2020, **18**, 9810–9815.

7 M. Camarasa, C. Barnils, R. Puig de la Bellacasa, J. Teixido and J. I. Borrell, A new and practical method for the synthesis of 6-aryl-5,6-dihydropyrido[2,3-*d*]pyrimidine-4,7(3*H*,8*H*)-diones, *Mol. Diversity*, 2013, **17**, 525–536.

8 I. Perez-Pi, X. Berzosa, I. Galve, J. Teixido and J. I. Borrell, Dehydrogenation of 5,6-dihydropyrido[2,3-*d*]pyrimidin-7(8*H*)-ones: A convenient last step for a synthesis of pyrido[2,3-*d*]pyrimidin-7(8*H*)-ones, *Heterocycles*, 2010, **82**, 581–591.

9 C. G. Bochet and A. Blanc, Photolabile protecting groups in organic synthesis, in *Handbook of Synthetic Photochemistry*, Wiley, 2010, vol. 13, pp. 417–447.

10 P. Klán, T. Šolomek, C. G. Bochet, A. Blanc, R. Givens, M. Rubina, V. Popik, A. Kostikov and J. Wirz, Photoremovable Protecting Groups in Chemistry and

Biology: Reaction Mechanisms and Efficacy, *Chem. Rev.*, 2013, **113**, 119–191.

11 N. Mont, J. Teixido, C. O. Kappe and J. I. Borrell, A one-pot microwave-assisted synthesis of pyrido[2,3-*d*]pyrimidines, *Mol. Diversity*, 2003, **7**, 153–159.

12 M. J. Hansen, W. A. Velema, M. M. Lerch, W. Szymanski and B. L. Feringa, Wavelength-selective cleavage of photoprotecting groups: strategies and applications in dynamic systems, *Chem. Soc. Rev.*, 2015, **44**, 3358–3377.

13 W.-L. Yu, Z.-G. Ren, K.-X. Ma, H.-Q. Yang, J.-J. Yang, H. Zheng, W. Wu and P.-F. Xu, Cobalt-catalyzed chemoselective dehydrogenation through radical translocation under visible light, *Chem. Sci.*, 2022, **13**, 7947–7954.

14 W. Jin and S. Yu, Photoinduced and palladium-catalyzed remote desaturation of amide derivatives, *Org. Lett.*, 2021, **23**(17), 6931–6935.

15 P. S. Sadhu, M. Ravinder, P. A. Kumar and V. J. Rao, Photochemical dehydrogenation of 3,4-dihydro-2-pyridones, *Photochem. Photobiol. Sci.*, 2009, **8**, 513–515.

16 W. Schilling, D. Riemer, Y. Zhang, N. Hatami and S. Das, Metal-Free Catalyst for Visible-Light-Induced Oxidation of Unactivated Alcohols Using Air/Oxygen as an Oxidant, *ACS Catal.*, 2018, **8**, 5425–5430.

17 V. Lloveras, P. Elías-Rodríguez, L. Bursi, E. Shirdel, A. R. Goñi, A. Calzolari and J. V. -Gancedo, Multifunctional Switch Based on Spin-Labeled Gold Nanoparticles, *Nano Lett.*, 2022, **22**, 768–774.

18 S. Zhang, V. Lloveras, S. Lope-Piedrafita, P. Calero-Pérez, S. Wu, A. P. Candiota and J. Vidal-Gancedo, Metal-Free Radical Dendrimers as MRI Contrast Agents for Glioblastoma Diagnosis: *Ex Vivo* and *In Vivo* Approaches, *Biomacromolecules*, 2022, **23**, 2767–2777.

19 F. A. Villamena, EPR Spin Trapping, in *Reactive Species Detection in Biology*, Elsevier, 2017, vol. 5, pp. 163–202.